A SELF-CONSISTENT MODEL ATMOSPHERE PROGRAM WITH APPLICATIONS TO SOLAR 0I RESONANCE LINES

by

R. Grant Athay and Richard C. Canfield*

High Altitude Observatory
National Center for Atmospheric Research
Boulder, Colorado

ABSTRACT

Profiles and total intensities are computed for solar 0I resonance lines at λ1302 and λ1305 using a model atmosphere program that includes non-LTE effects in both hydrogen and oxygen and that includes microturbulence both as a line broadening mechanism and as a contribution to the gas pressure. Good agreement is obtained between computed and observed intensities. The computed profiles appear to have too much self-reversal.

Key words: resonance lines, non-LTE line formation, solar UV lines.

I. INTRODUCTION

The development of adequate methods for computing profiles and intensities of strong stellar lines where non-LTE (local thermodynamic equilibrium) effects are of overriding importance has provided a powerful new means for studying the outer envelopes of extended stellar atmospheres. In principle, at least, such studies are capable of yielding thermodynamic models and the statistical characteristics of the fluid motions at the depths where the lines are formed. In practice, we are barely beginning

*Currently at Utrecht Observatory.

https://doi.org/10.1017/S0252921100151188 Published online by Cambridge University Press

to make use of such methods, partly because we are still developing the diagnostic techniques and partly because we still lack adequate data.

The solar chromosphere provides an excellent proving ground for the development of the diagnostic methods of the non-LTE approach to line formation. Although the thermodynamic and hydrodynamic state of the chromosphere are known only approximately, a few properties of the chromosphere and its adjacent layers are known with relatively high precision. Eclipse data, for example, provide spatially averaged values of the quantity $\langle n_e n_p T^{-3/2} \rangle$, where n_e = electron density, n_p = proton density, and T = electron temperature, that are accurate to about a factor of two in the height range 500 km to 2500 km above the solar limb. It is not known exactly what the "average" refers to, but present evidence indicates that at depths near 500 km the chromosphere is not grossly inhomogeneous. Thus, one may assume that the eclipse value of $\langle n_e n_p T^{-3/2} \rangle$, a quantity we shall subsequently denote by EPT, is representative of the mean chromosphere near 500 km. Above about 1000 km the chromosphere is evidently dominated by inhomogeneities (such as spicules) and the value of EPT is not representative of the mean chromosphere. Below 500 km EPT is not well known.

The known values of EPT near 500 km provide very useful checks on model atmosphere calculations. Additional valuable boundary conditions are provided by photospheric models and coronal models, which are reasonably well known. It seems well established, for example, that in the low corona the electron density is of the order 3×10^8 cm^{-3} and the electron temperature is of the order of 2×10^6 °K. Assuming that $n_p = n_e$, we find that the gas pressure in the low corona is approximately 0.2 dyne cm^{-2}. The gas pressure at a continuum ($\lambda 5000$) optical depth, τ_o, of 10^{-5}, which corresponds to a geometrical height of about 500 km above the limb, is of the order of 2×10^2 dyne cm^{-2}. Thus, the gas pressure decreases by a factor of only about 10^3 between a height of 500 km in the chromosphere and the base of the corona. Within this same interval T increases from about 6000°K to 2×10^6°K.

In addition to the stronger Fraunhofer lines that are formed in the chromosphere, profiles are available for the Lyman-α and Lyman-β lines of hydrogen and for the C II line at λ1336 (Berger and Bruner[1]) and the OI lines at λ1302 and λ1305 (Bruner and Rense[2]). The OI lines are of interest in that they are formed in the middle chromosphere where the

quantity EPT is reasonably well known.

Oxygen and hydrogen have similar ionization potentials and similar excitation potentials for their respective resonance lines. This leads to the result that the two atomic species ionize at the same depths in the atmosphere. The ionization of hydrogen largely determines both the mean molecular weight in the atmosphere and the electron density and therefore critically influences the model atmosphere. In addition, part of the ionization of 0I is produced by the Lyman continuum radiation of hydrogen. It is necessary, therefore, to solve the ionization equilibrium and Lyman continuum radiative transfer problems for hydrogen in order to compute profiles of the 0I lines.

II. CONSTRUCTION OF SELF-CONSISTENT MODEL CHROMOSPHERES

We propose to compute a model chromosphere using a minimum number of arbitrary parameters, i.e., we maximize the constraints on the model. The constraints exercised are the following:

1. The quantity $n_e n_p T^{-3/2}$ = EPT given by the model must agree within a factor of two with eclipse values derived by Henze[3] in the height range 500-1000 km, and it must not exceed the eclipse values at heights above 1000 km.
2. The gas pressure in the chromosphere must exceed 0.2 dyne cm^{-2}.
3. At height zero, i.e., at the limb as defined by a tangential continuum opacity of unity at $\lambda 5000$, we adopt T = 4600° and a hydrogen density, n_H of 1.6×10^{16}.
4. We assume that the hydrostatic equation

$$dp = - \rho g \, dh \qquad (1)$$

is valid and that

$$p = nkT + \frac{1}{3} \zeta^2 \Sigma n_i m_i \quad , \qquad (2)$$

where ζ is the microturbulent velocity and n_i and m_i are the number density and mass of particles of type i. The other symbols have their usual meaning. We

https://doi.org/10.1017/S0252921100151188 Published online by Cambridge University Press

adopt a helium:hydrogen number density ratio of 1:10.

5. We require that the flux in the Lyman continuum produced by the model chromosphere be within fifty percent of the value reported by Noyes and Kalkofen[4].

With these constraints there is very little freedom in the temperature model, but there is essentially complete freedom in $\zeta(\tau)$.

Equation (2) may be rewritten in the form

$$p = nkT\ F \tag{3}$$

where

$$F = 1 + \frac{\zeta^2 \sum_i n_i m_i}{3nkT} \quad . \tag{4}$$

Also, we may write

$$\rho = 1.4\ n_H m_H \quad , \tag{5}$$

$$n = 1.1\ n_H + n_e \quad , \tag{6}$$

and

$$I = \frac{n_H}{n_H + n_e} \quad , \tag{7}$$

where n_H is the number of neutral hydrogen atoms plus protons and m_H is the hydrogen mass. Equations (1) and (3) then yield

$$d\ell n\ (1.1\ n_H + n_e) = -\ d\ell n\ T - \frac{1.4\ m_H\ g\ I}{k\ F\ T\ (1+0.1I)}\ dh \quad . \tag{8}$$

The ionization parameter I has limits $0.5 \leq I \leq 1$ and can be determined for a given model atmosphere only by solving the radiative transfer equations for the Lyman continuum. The transfer solutions depend upon n_e and n_H as well as T_e. Thus, we must proceed iteratively to find a self-consistent solution. We start by assuming T(h), F(h) and I(h). We then solve equation (8) to obtain preliminary

https://doi.org/10.1017/S0252921100151188 Published online by Cambridge University Press

values of $n_H(h)$ and $n_e(h)$. We use these initial values, denoted by $n_H(1)$ and $n_e(1)$ to obtain initial values of all collision and recombination rates and initial values of τ in the Lyman continuum. Since τ depends upon n_1, the ground state population, and n_1 depends upon τ through the transfer equation, the transfer equation must be solved iteratively with n_1 to obtain consistent values of $n_1(1)$ and τ. The converged values of $n_1(1)$ are then combined with $n_H(1)$ to give $n_e(1')$ and $I(2)$. From $I(2)$ we obtain $n_H(2)$ and $n_e(2)$ from equation (8) and repeat the iteration on τ and n_1. This double iterative procedure is continued until final convergence is achieved for τ, n_H, n_1 and n_e.

For an arbitrary choice of $T(h)$ and $F(h)$, we do not satisfy the constraints (1), (2) and (5). Hence, for a given $F(h)$, we must adjust $T(h)$ until the constraints are satisfied. Each change in either $T(h)$ or $F(h)$ requires a new iterative solution for n_H, n_1 and n_e.

We have constructed by this technique twelve self-consistent model atmospheres. Most of the ionization of hydrogen occurs in the regions where Lyman continuum transfer is important and where the Lyman lines are in radiative detailed balance. Hence, it is not essential to consider the transfer problem in the Lyman lines. Furthermore, most of the ionizations in hydrogen occur from the n_2 level, which is populated mainly from the n_1 level, and a fairly accurate solution is obtained using a model atom with two bound energy levels plus a continuum.

III. LYMAN CONTINUUM TRANSFER SOLUTIONS

In treating the Lyman continuum problem we make the following simplifying assumptions: (1) There is no opacity other than Lyman continuum opacity from $\lambda 912$ to approximately $\lambda 450$. (2) Stimulated emissions may be ignored. (3) Lyman-α is in radiative detailed balance, and we ignore bound levels above n=2. (4) The scattering is non-coherent.

It is convenient to work with the b_n parameters rather than energy level populations. The Lyman continuum source function for the problem we are considering is

$$S_\nu = \frac{2h\nu^3}{c^2} \quad \frac{e^{-h\nu/kt}}{b_1} \quad . \tag{9}$$

https://doi.org/10.1017/S0252921100151188 Published online by Cambridge University Press

The only unknown in this equation is b_1 . We could, therefore, formulate the problem in such a way as to solve for b_1^{-1} or the product of b_1^{-1} and any known function. For convenience, we define a dimensionless frequency parameter y such that

$$y = \frac{\nu}{\nu_1} \tag{10}$$

where ν_1 is the frequency at the Lyman limit. We may then write

$$S_y = y^3 \exp - \left[h\nu_1(y-1)/kT\right] S_1, \tag{11}$$

where

$$S_1 = \frac{2h\nu_1^3}{c^2} \frac{e^{-h\nu_1/kT}}{b_1} . \tag{12}$$

This divides S_y into two factors, one frequency dependent and one frequency independent. We shall formulate the transfer equation to solve for the frequency independent term, S_1.

It follows from the equations of statistical equilibrium and from the frequency dependence of the photoionization cross section for hydrogen that

$$S = \frac{\frac{e^{-h\nu_1/kT}}{E_1} \int_1^\infty \frac{J_y}{y^4} dy + \varepsilon^* B_1}{1 + \varepsilon^\dagger} , \tag{13}$$

where

$$E_1 = \int_{\nu_1}^\infty \frac{e^{-h\nu/kT}}{\nu} d\nu , \tag{14}$$

J_y = mean intensity,

B_1 = Planck function at y = 1 ,

https://doi.org/10.1017/S0252921100151188 Published online by Cambridge University Press

$$\varepsilon^* = \varepsilon + \frac{R_{12}\, R_{2C}}{W_C A_{C1} R_{22}} \quad , \tag{15}$$

$$\varepsilon^\dagger = \varepsilon + \frac{R_{21}\, R_{C2}}{W_C\, A_{C1}\, R_{22}} \quad , \tag{16}$$

$$\varepsilon = \frac{C_{C1}}{A_{C1}} = \frac{\text{collisional recombination rate}}{\text{radiative recombination rate}} \quad ,$$

$$R_{ij} = W_i\, P_{ij} = \tilde{\omega}_i\, e^{-h\nu_i/kT}\, P_{ij} \quad ,$$

$\tilde{\omega}_i$ = statistical weight of level i,

$h\nu_i$ = energy of level i measured from the ground state,

P_{ij} = transition rate i to j,

P_{ii} = sum of all rates out of level i.

We write the transfer equation in the flux derivative form

$$\frac{dH_y}{d\tau_y} = J_y - S_y \tag{17}$$

and eliminate the term in J_y from equations (17) and (13). From equation (17), we have

$$\frac{e^{-h\nu_1/kT}}{E_1} \int_1^\infty \frac{J_y}{y^4}\, dy = \frac{e^{-h\nu_1/kT}}{E_1} \int_1^\infty \frac{1}{y^4} \frac{dH_y}{d\tau_y}\, dy + S_1 \quad . \tag{18}$$

https://doi.org/10.1017/S0252921100151188 Published online by Cambridge University Press

It follows from equation (13) that

$$S_1 = \frac{\varepsilon^* B_1}{\varepsilon^\dagger} + \frac{e^{-h\nu_1/kT}}{\varepsilon^\dagger E_1} \int_1^\infty \frac{1}{y^4} \frac{dH_y}{d\tau_y} \, dy \ . \tag{19}$$

In symbolic form, equation (17) gives

$$\frac{dH_y}{d\tau_y} = J_y - S_y = (\Lambda - I)S_y \quad , \tag{20}$$

where Λ is the mean intensity operator and I is the unit operator. Using equation (11), we may rewrite equation (20) as

$$\frac{dH_y}{d\tau_y} = y^3 \left\{(\Lambda - I) \exp - \left[h\nu_1(y-1)/kT\right]\right\} S_1 \tag{21}$$

$$= y^3 \, \Phi \, (y,\tau) \, S_1 \quad . \tag{22}$$

Thus, we have finally

$$S_1 = \frac{\varepsilon^* B_1}{\varepsilon^\dagger} + \frac{e^{-h\nu_1/kT}}{\varepsilon^\dagger E_1} \int_1^\infty y^{-1} \, \Phi \, (y,\tau) S_1 \, dy \quad . \tag{23}$$

This equation is solved by the method of Athay and Skumanich[5] by writing

$$S_1 = (1 - \alpha)^{-1} \frac{\varepsilon^* B_1}{\varepsilon^\dagger} \quad , \tag{24}$$

where α is a matrix operator defined by

$$\alpha = \frac{e^{-h\nu_1/kT}}{\varepsilon^\dagger E_1} \int_1^\infty y^{-1} \, \Phi \, (y,\tau) \, dy. \tag{25}$$

https://doi.org/10.1017/S0252921100151188 Published online by Cambridge University Press

The y and τ spaces are discretized into 9 points in y between y = 1 and y = 2 and 42 points in τ. We have tried increasing the number of y points and increasing the range in y to y = 3. Neither change produces significant changes in S_1.

The iterative process of solving equations (8) and (25) to obtain self-consistent solutions for a given T(h) and F(h) generally requires 13 iterations. The complete program requires approximately 3 minutes on a CDC 6600. The solutions appear to be very stable even when large gradients in T(h) and F(h) are introduced.

The assumption that Lyman-α is in detailed balance is not necessary of course. The problem could be solved by including transfer solutions in Lyman-α, but trial calculations showed that this greatly increases the number of iterations required and did not result in any important changes in the model atmosphere for the region of interest for the 0I lines.

IV. CHARACTERISTICS OF MODELS

Constraint (1) from Section II effectively fixes T(h) between 500 and 1000 km subject somewhat to the assumed form of F(h). However, it follows from equation (4) that the ratio of ζ to the mean thermal velocity of hydrogen atoms is given by

$$\frac{\zeta}{V(H)} = 1.04\ (F-1)^{1/2}\ (1.1 + \frac{n_e}{n_H})^{1/2} \quad . \qquad (26)$$

Thus, if $n_e/n_H \ll 1$, $\zeta/V(H) = .5$ for $F \approx 1.2$ and $\zeta/V(H) = .75$ for $F \approx 1.5$. In the low chromosphere ζ is a few km/sec at most, and F is therefore close to unity. In the mid-chromosphere even if we want $\zeta \approx 10$ km/sec, which is larger than required for the 0I lines, we need only $F \approx 1.5$. In practice, therefore, we cannot change F(h) very much without introducing unreasonable values of ζ.

Between heights of zero and 500 km we have adopted a rather arbitrary model for T(h) and we have set F = 1. The T(h) model has a slow rise in T to 4700°K at 200 km followed by a more rapid rise to 5200°K at 400 km and $\approx$ 5600°K at 500 km. The

https://doi.org/10.1017/S0252921100151188 Published online by Cambridge University Press

value of T at 500 km is dictated by the eclipse value of $n_e\ n_p\ T^{-3/2}$ at that height. It would make little difference to the model at 500 km and higher if, for example, we decreased T to 4000°K at 200 km followed by a rapid rise to $\approx$ 5600°K at 500 km. This would effectively change the density scale height by about 20 percent for one scale height and would result in a small density decrease at 500 km. The constraints we have set on the model do not, therefore, lead to any practical restrictions on the temperature minimum region.

Between 500 km and 1000 km constraint (1) imposes a gradual rise in T to $\approx$ 6200° at 1000 km (cf. Athay[6]). If T is constant in this height interval the computed values of EPT decreases much too rapidly with height. If T increases only somewhat more rapidly than indicated EPT increases with height.

The reason for the strong sensitivity to T in the height interval 500-1000 km results from the fact that hydrogen is still only partially ionized. In fact at 1000 km hydrogen is only about 2 percent ionized. The ionization does not reach the 50 percent level until T reaches about 8000°K. This again means that constraint (1) limits the kinds of models that may be considered. A rapid increase of T with height cannot be permitted in a model of the mean chromosphere at depths where $T \lesssim 8000°$ without introducing an increase in EPT with height, which is unacceptable.

At 1000 km the gas pressure in the chromosphere is approximately 7 dyne cm^{-2}. Therefore, constraint (2) becomes very important in determining the nature of the model at heights above 1000 km. The gas pressure cannot fall by more than a factor of 40 before the coronal temperature rise occurs, and a sharp temperature rise cannot occur until $T \gtrsim 8000°$. This requires that T continue to rise rather gradually until it reaches about 8000°.

We have somewhat arbitrarily adopted a T(h) distribution above 1000 km that gives $d \log_{10} T/dh \approx 10^{-9}$ cm^{-1} up to $T \approx 7200°$. This is the same gradient that exists between 500 and 1000 km, and is about the maximum gradient allowed by EPT. The value T = 7200° is reached at approximately 1600 km and the gas pressure has decreased to about 0.5 dyne cm^{-2}. If we continued increasing T at this same rate, the gas pressure would reach 0.2 dyne cm^{-2} before T reached 8000°. It is necessary, therefore, to steepen the gradient in T between 7200° and 8000°. Hydrogen is sufficiently ionized at 7200° to permit

a steepening of the temperature gradient without making EPT too large. The larger T becomes the more the gradient may be steepened.

Restrictions on d $\log_{10}$ T/dh are also imposed by constraint (5) - the observed Lyman continuum intensity. The type of model under consideration tends to give too much flux in the Lyman continuum. Steepening the temperature gradient between T = 7500° and T = 10000° reduces the Lyman continuum flux to within the limits set by constraint (5).

A model that satisfies all of the constraints in Section II is given in Table 1. It is possible to construct a family of such models with different assumed values for F(h). Such models differ from one another primarily in the height at which the sharp temperature rise occurs. The differences amount to only a few hundred kilometers, however, even for relatively large changes in ζ.

A total of 12 models were tested by comparing computed and observed profiles for the 0I lines. Each of the 12 models gave Lyman continuum intensities within a few percent of the observed values and each gave total intensities in the 0I lines that agreed within a factor of two with the intensities observed by Hinteregger[7]. The model in Table 1 gave the best agreement with the 0I profiles. Details of the oxygen calculations are discussed in the following sections.

V. OXYGEN TRANSFER SOLUTIONS

Source functions for the resonance lines of 0I are computed using the technique described by Athay and Canfield[8] for the Mg b and Na D lines. The 0I transitions occur between $2p^4\ {}^3P$ and $3s\,{}^3S^o$. There appears to be no interlocking transitions of importance other than transitions to and from the continuum. This conclusion was reached after trial calculations that included $3s\,{}^5S^0$, $3p\,{}^5P^o$ and $3p\,{}^3P$ levels showed that the source functions for the resonance triplet were essentially the same as when these levels were omitted.

Both ionization and recombination occur mainly from and to the ground state, $2p^4\ {}^3P$. Also, the ground state serves as the primary source of electrons for the $3s\,{}^3S^o$ level. This accounts for the lack of important interlocking levels.

Photoionization rates from the $2p^4\ {}^3P$ level are computed using the Lyman continuum intensities computed for the model atmosphere and photoionization

https://doi.org/10.1017/S0252921100151188 Published online by Cambridge University Press

TABLE 1

MODEL CHROMOSPHERE

Height (km)	T	log n_H	log n_p	log n_e	log n_2	b_1	b_2	log P	F	ζ (km/sec)
0	4600	16.20	10.56	12.20	5.61	.24	.24	4.04	1.0	0
200	4700	15.42	10.73	11.49	5.06	.30	.30	3.28	1.0	0
400	5200	14.62	11.20	11.32	5.32	.73	.73	2.52	1.0	0
550	5700	14.08	11.42	11.45	5.65	1.5	1.5	2.00	1.0	0
700	5900	13.63	11.36	11.36	5.50	2.0	2.0	1.59	1.1	3.5
1000	6250	12.84	11.23	11.23	5.20	3.1	3.1	.83	1.15	4.5
1200	6500	12.38	11.14	11.14	5.04	4.0	4.0	.40	1.2	5.3
1500	7000	11.74	11.08	11.08	4.89	6.4	6.7	-.23	1.3	7.1
17 0	7600	11.23	10.88	10.88	4.49	22	11	-.57	1.3	8.0
1935	8400	10.97	10.66	10.66	4.04	260	21	-.70	1.3	8.6
1975	9250	10.87	10.59	10.59	3.92	1900	40	-.82	1.3	9.1
1983	10400	10.79	10.59	10.59	3.98	1.1×10^4	97	-.82	1.3	10
1998	14900	10.54	10.52	10.52	4.00	1.7×10^5	700	-.82	1.3	13
2007	20200	10.40	10.40	10.40	3.65	6.6×10^5	1800	-.82	1.3	15

https://doi.org/10.1017/S0252921100151188 Published online by Cambridge University Press

cross sections measured by Cairnes and Samson[9]. For the $3s\ ^3S^o$ photoionization rates we use a cross section equal to $.19\pi a_o^2\ (\nu_o/\nu)^3$ obtained from the Burgess and Seaton[10] quantum defect method together with quantum defects computed by Peach[11]. We use a solar radiation temperature of 5350° to give the mean intensity for photoionization.

Transition probabilities for the resonance triplet are obtained from Σ gf = .19 as given by Parkes, Keyser, and Kaufman[12]. Electron collisional excitation cross sections, Q_{ij}, are not well known for 0I. We adopt a mean value of $Q = .1\pi a_o^2$ for each of the resonance transitions (cf. Stauffer and McDowell[13]). However, we vary this Q to ascertain its effect upon the 0I lines. For transitions between J substates of $2p^4\ ^3P$ we use $Q = 10\pi a_o^2$. Collisional ionization rates are unimportant. However, we use $Q = .15\pi a_o^2$ for ionizations from $2p^4\ ^3P$ and $Q = 7.5\pi a_o^2$ for ionizations from $3s\ ^3S^o$.

The source functions for the triplet are evaluated iteratively. Stimulated emissions are ignored and the scattering is assumed to be non-coherent. We adopt an oxygen abundance of 6×10^{-4}.

The three members of the 0I triplet appear to be of about equal intensity, .01 ergs cm^{-2} sec^{-1} at the orbit of earth (Hinteregger[7]). Assuming that the intensity is relatively uniform across the solar disk, we find a flux at the center of the solar disk of approximately 35 ergs cm^{-2} sec^{-1} $ster^{-1}$.

Computed intensities of the 0I lines are sensitive to the model atmosphere, to the oxygen abundance, to the gf values, and to line broadening parameters. However, they are not particularly sensitive to the collisional excitation cross section. For example, an increase in Q by a factor of four for each of the triplet lines increases the line intensity by a factor of approximately 1.5 only (see Table 2).

The chromosphere is effectively thick in the 0I triplet and the line intensities are proportional to the product of the degradation length, τ_{deg}, and the mean source term for photon generation $\langle \varepsilon^* B \rangle$ in the layer $0 \leq \tau \leq \tau_{deg}$. An increase in the collisional excitation cross section increases ε^* and decreases τ_{deg}. The two effects nearly cancel.

The line broadening parameters affect τ_{deg}, and hence the line intensities. We have used a Voigt profile with both radiation and collision damping. Since the cross section for collision damping is not accurately known, we pick a value for the collision damping half width that gives best agreement with

https://doi.org/10.1017/S0252921100151188 Published online by Cambridge University Press

TABLE 2

LINE FLUXES (ergs sec^{-1} cm^{-2} $ster^{-1}$) AND RATIOS OF PEAK INTENSITY TO CENTRAL INTENSITY FOR λ1302 AND λ1305

line		λ1302		λ1305	
Q	VW	Flux	Peak:Center	Flux	Peak:Center
	1	17	2.6	16	2.3
.1	3	24	2.7	22	2.2
	10	39	3.1	37	2.7
	1	25	2.2	23	2.1
.4	10	60	2.5	56	2.2
	30	41	2.4	40	2.6

the observed profile. The adopted form for the half width in angstroms is 6.4×10^{-21} n_H (VW) where the parameter VW may take on different values. The value of VW affects the intensity of the line as well as its profile. Intensities of the λ1302 and λ1305 members of the multiplet are given in Table 2 as a function of VW and the electron excitation cross section Q. The intensities would be influenced also by changes in the gf values.

The shapes of the wings of the lines depend upon the damping parameters and can be fitted reasonably well by adjusting VW. The shapes of the Doppler cores of the lines depend upon both the magnitude and gradient of ζ. In general, the computed profiles show strong self reversal whereas the observed profiles show weak self-reversal. The amount of self-reversal in the computed profiles decreases as $d\zeta/dh$ is increased. However, it does not appear to be possible to obtain complete agreement between observed and computed profiles without excessively large values of $d\zeta/dh$. The self-reversal is not markedly sensitive to either the collision damping or the collisional excitation cross section as evidenced by the ratios of peak intensity to central intensity given in Table 2.

https://doi.org/10.1017/S0252921100151188 Published online by Cambridge University Press

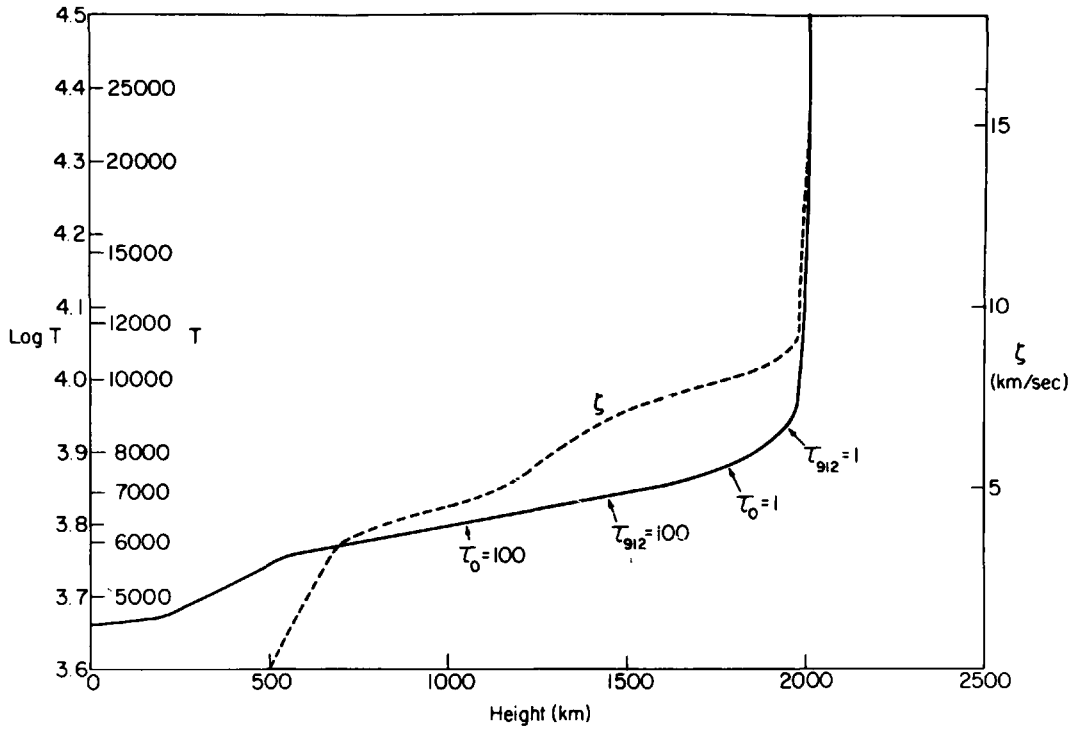

Figure 1. A temperature model deduced from the constraints in Section IV and a $\zeta(h)$ model that gives best agreement with the position of peak intensity and the ratio of peak intensity to central intensity in the OI lines. The optical depth at the center of λ1305 is indicated by τ_0, and the optical depth at the head of the Lyman continuum is indicated by τ_{912}.

Figure 1 exhibits $\zeta(h)$ and $T(h)$ from Table 1. Figure 2 exhibits the λ1305 profile computed from the model in Table 1 for three values of VW together with an observed profile. The observed profile shown is reduced from observations by Bruner and Rense[2]. Improved observations have been made with increased spectral resolution and are in process of reduction at the time of this writing. It does not appear that the improved profiles will differ greatly from the one shown. The source function for the λ1305 line and the non-LTE departure coefficients for the ground state, b_1, and the 3s $^3S^o$ level, b_3, are shown in Figure 3. A more complete tabulation of the OI calculations is given in Table 3. The adopted collision cross section between different J states in the ground level is sufficiently large to give relative populations that conform very nearly to a Boltzmann distribution.

Although the computed and observed profiles do not show good agreement near line center there are several possible explanations. The sharp emission

https://doi.org/10.1017/S0252921100151188 Published online by Cambridge University Press

TABLE 3

OXYGEN CALCULATIONS

Height (km)	τ_o(1305)	S(1305)	S(1302)	log n ($2p^4\ ^3P$,J=1)	log n_o ($3s\ ^3S^o$)	b ($2p^4\ ^3P$,J=1)	b_o ($3s\ ^3S^o$)
0	1×10^5	1.4×10^{-11}	1.4×10^{-11}	11.91	1.80	.27	.43
200	3.2×10^4	3.0	3.0	11.43	1.65	.32	.65
400	6.1×10^3	31	30	10.63	1.75	.88	1.26
550	8.2×10^2	82	82	9.74	1.40	2.2	1.33
700	5.0×10^2	89	89	9.47	1.14	2.5	1.20
1000	1.5×10^2	91	90	8.94	.65	3.4	.80
1200	79	86	86	8.77	.45	3.6	.57
1500	19	58	64	8.30	-.16	4.6	.24
1770	6.0	32	35	7.77	-.96	6.9	.089
1935	1.6	18	19	7.40	-1.60	14	.043
1975	.41	12	11	6.97	-2.22	80	.050
1983	.067	9.0	8.4	6.83	-2.48	790	.11
1998	.013	13	13	6.56	-2.56	9.8×10^4	.84
2007	.0043	35×10^{-11}	35×10^{-11}	6.34	-2.37	1.7×10^6	5.6

https://doi.org/10.1017/S0252921100151188 Published online by Cambridge University Press

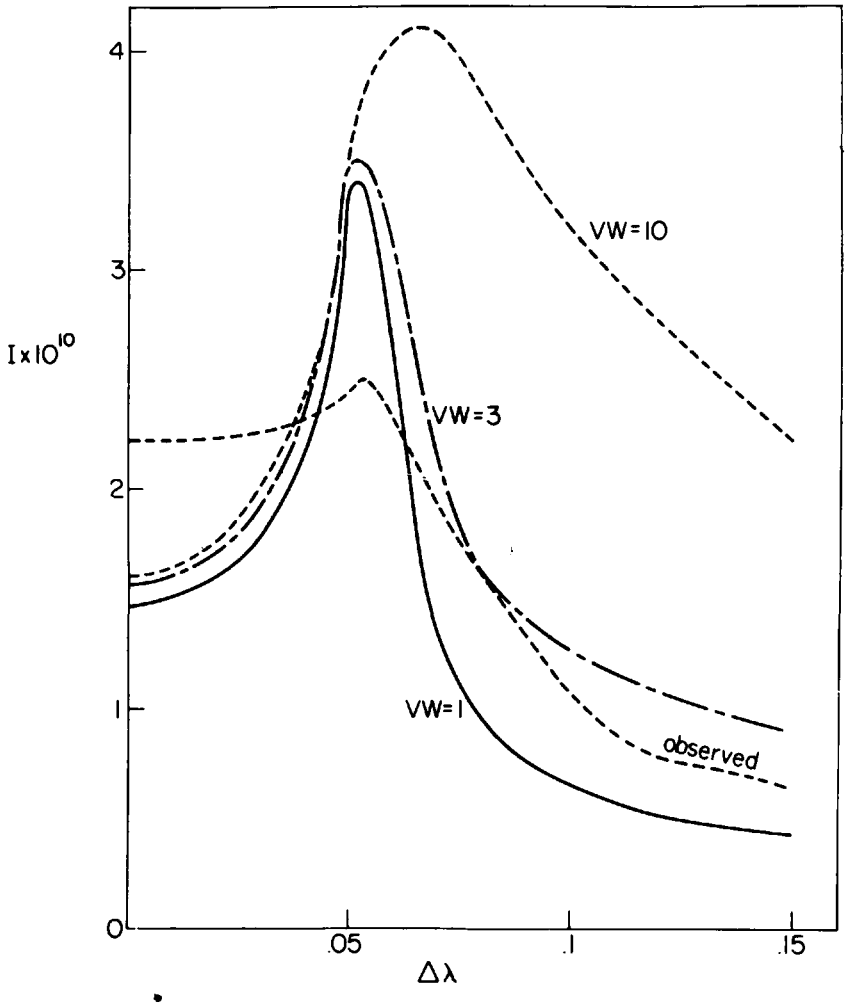

Figure 2. Comparison of observed λ1305 profile (preliminary reduction, see text for explanation) and computed profiles for VW = 1, 3 and 10.

peak in the computed profiles at the edge of the Doppler core has a width of the same order as the instrumental resolution and is perhaps partially "lost" in the observed profile. Also, macroturbulence and atmospheric inhomogenieties may substantially alter the "average" profile observed with low spatial resolution.

The tendency for non-LTE source functions to give central intensities that are somewhat lower than observed appears to be a common difficulty. In computations of Mg II and Ca II profiles (Athay and Skumanich[14]) and Na D profiles (Athay and Canfield[8]) it has been necessary to resort to rather large values of $d\zeta/dh$ in order to obtain central intensities as large as those observed. Broadly speaking, the values of ζ in Table 1 and Figure 1 are consistent with values obtained from the Ca II and Na D lines. The 0I lines are formed

https://doi.org/10.1017/S0252921100151188 Published online by Cambridge University Press

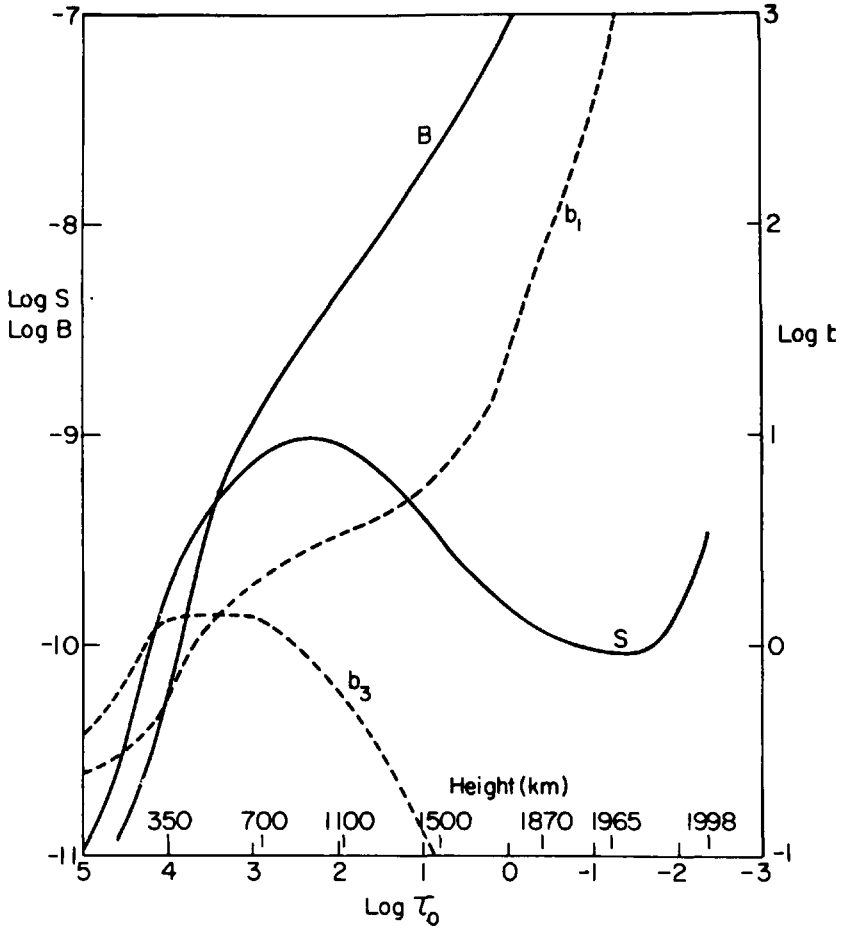

Figure 3. Source function and non-LTE departure coefficients for λ1305. Source functions for the other two members of the triplet are closely equal to the λ1305 source function (see Table 3).

somewhat higher than the Ca II lines, but the Doppler cores of these lines are strongly overlapped in their depths of formation. It should be possible to combine analyses of the Na D, Ca II, Mg II, and OI lines to obtain a single $\zeta(h)$ model provided the concept of a spherically symmetric chromosphere has a valid meaning in this context at the depths where the lines are formed. Additional help will come from analysis of C II profiles recently observed by Berger and Bruner[1].

The authors are indebted to W. Frye for most of the programming and computing and especially to W. A. Rense and E. Bruner for allowing them the use of the OI profiles prior to publication.

REFERENCES

1. R. A. Berger and E. C. Bruner, Jr. 1969, *Ap. J.* 155, L115.
2. E. C. Bruner, Jr., and W. A. Rense 1969, *Ap. J.*, in press.
3. W. B. Henze 1968, Thesis, Univ. of Colorado, Boulder (also Solar Physics, in press).
4. R. W. Noyes and W. Kalkofen 1969, Paper presented at Solar Physics Meeting of AAS, Pasadena.
5. R. G. Athay and A. Skumanich 1967, *Ann. d'Ap.* 30, 669.
6. R. G. Athay 1969, *Solar Physics*, in press.
7. H. E. Hinteregger 1965, *The Solar Spectrum*, Ed. C. de Jager (Reidel: Dordrecht), 179.
8. R. G. Athay and R. C. Canfield 1969, *Ap. J.* 156, 000.
9. R. B. Cairnes and J. A. R. Samson 1965, *Phys. Rev.* 139, A1403.
10. A. Burgess and M. Seaton, 1960 *M.N.* 120, 121.
11. G. Peach 1962, *M.N.* 124, 371.
12. D. A. Parkes, L. F. Keyser and F. Kaufman 1967, *Ap. J.* 149, 217.
13. A. D. Stauffer and M. R. C. McDowell 1966, *Proc. Phys. Soc. Lon.* 89, 289.
14. R. G. Athay and A. Skumanich 1968, *Solar Physics* 3, 181.

DISCUSSION

Thomas: You find a very steep temperature rise for $\tau_{912} = 1$. How is the fit of other observation such as the Balmer and Paschen jump? Can you explain the observed helium lines? Also, I worry at your neglect of Hα in solving the LyC transfer problem. Including it, as I did in the chromosphere book we wrote, will raise b_1, b_2, T_e, dT_e/dh if that solution is a guide.

Athay: If I change the microturbulence and the pressure gradient I shall get the increase of temperature at smaller heights and the observations fit very well. The helium lines can be explained if you take an asymmetric atmosphere.

Mugglestone: Are your results very sensitive to the dependence of microturbulence with height?

Athay: The increase of turbulence has different effects. It makes the line broader, increases the

https://doi.org/10.1017/S0252921100151188 Published online by Cambridge University Press

central intensity, and it decreases the intensity of the emission. The observed relation of emission to absorption is 2:1.

Underhill: The resolution of the observed spectra is low, of the order of 20 or 5A.

Athay: There are new observations with a resolution of 0.015A (Bruner and Rense Ap. J. 157, 417, 1969). But even with this resolution you cannot observe the reversal in the line center with sufficient accuracy. We do find similar problems with reversal in the line centers for Lyα, Ca II K and Na I D lines.

Kalkofen: What about Lyβ?

Athay: Lyβ is very weak. The Ly-continuum is strong, approximately 10 times the intensity of Lyα; Lyβ has only 1% of the intensity of Lyα.

Kalkofen: Did you test your theory with observed lines of high excitation and with the observed center to limb variations?

Athay: We find agreement within a few percent with the observed limb darkening and limb brightening.

Wellmann: If one observes OI lines in stellar spectra and can do a temperature determination with these lines, can you say in which layer the lines are formed?

Athay: No.

https://doi.org/10.1017/S0252921100151188 Published online by Cambridge University Press